### **Research Article**

Mohammed S. Alqahtani, Rabbani Syed\*, Mudassar Shahid, and Jilani Purusottapatnam Shaik

# Synthesis and characterization of ZnO/β-cyclodextrin/nicotinic acid nanocomposite and its biological and environmental application

https://doi.org/10.1515/gps-2023-0050 received March 23, 2023; accepted May 31, 2023

Abstract: In the present work, the disk-shaped zinc oxide (ZnO) nanoparticles were synthesized and functionalized with  $\beta$ -cyclodextrin ( $\beta$ -CD) and nicotinic acid (vitamin B3) using the wet co-precipitation method. The functionalized ZnO/β-CD/nicotinic acid nanocomposite materials were characterized using UV-visible spectroscopy (UV-Vis), Fourier transform infrared (FTIR) spectroscopy, X-ray diffraction (XRD), energy dispersive spectroscopy (EDS), field emission electron microscopy (FESEM), and band-gap energy analysis. The band gap value  $(E_g)$  was 4.3 eV. The average XRD crystallite size was determined using the Scherrer formula and was found to be 50 nm. The ZnO/β-CD/nicotinic acid nanocomposite material showed a photocatalytic effect for dye-polluted wastewater. It also showed an antibacterial effect against the Gram-positive bacterial strain Streptococcus aureus (S. aureus) but did not show any antibacterial activity with Gram-negative Escherichia coli (E. coli). The ZnO/β-CD/nicotinic acid nanocomposite also showed antifungal activity with Aspergillus niger (A. niger). It was noticed that ZnO/β-CD/nicotinic acid nanocomposite showed efficient anticancer activity with  $IC_{50} = 14.95 \,\mu\text{g}\cdot\text{mL}^{-1}$  in MCF-7 cell lines. Because of the formation of singlet oxygen (O2-) and hydrogen oxide radical (-OH'), the composite material showed a photodegradation reaction against aq. solution of methylene blue dye. After 190 min, the blue colour of aq. solution methylene blue was decolourized at 6 pH at a constant time interval.

**Keywords:**  $ZnO/\beta$ -cyclodextrin/nicotinic acid nanocomposite material, wastewater, antibacterial property, antifungal activity, anticancer

# 1 Introduction

In the last few years, nanomaterials are used in almost every field including drug delivery [1], sensors and photonic devices [1], electro-catalytic degradation of dyes, removal of metal ions [2-4], energy storage, etc. Because of environmental friendliness as well as unique electrical, optoelectronic, photochemical, catalytic, and biomedical [5] properties, zinc oxide (ZnO) nanomaterials were extensively used [6-9]. ZnO, one of the earliest materials, was used as a gas sensor because of the high mobility of conduction electrons in the material and good chemical and thermal stability [10,11]. ZnO nanomaterials also attract interest because of their wide range of applications [12,13]. They had a wide band energy gap and are used in electronics, semiconductors, and sensor technology [14,15]. Recently, Cu-ZnO nanocomposite materials played an important role under reduced reaction conditions [16].

The ZnO nanomaterials were synthesized by different synthetic methods like sol–gel technique [17,18], microemulsion process [19], mechano-chemical process [20], spray pyrolysis and drying process [21], plasma synthesis [22], hydrothermal process [23], sonochemical or microwave synthesis [24,25], direct precipitation process [26], etc. However, due to the presence of water, the formation of Zn–O–Zn bonds and hard agglomerates in the nanomaterial impede applications of ZnO nanomaterials. Thus, the reduction of water from the nanomaterial is an important process for reducing hard agglomerates. Nowadays, water pollution has increased due to the contamination of non-biodegradable pollutants from many industries [27].

Today, the most common water pollutants are organic dyes, which affect the photosynthesis process and also cause medical conditions like skin irritation, allergy,

**Mohammed S. Alqahtani, Mudassar Shahid:** Department of Pharmaceutics, College of Pharmacy, King Saud University, P.O. Box 2457, Riyadh, 11451, Saudi Arabia

**Jilani Purusottapatnam Shaik:** Department of Biochemistry, College of Science, King Saud University, Riyadh, Saudi Arabia

<sup>\*</sup> Corresponding author: Rabbani Syed, Department of Pharmaceutics, College of Pharmacy, King Saud University, P.O. Box 2457, Riyadh, 11451, Saudi Arabia, e-mail: rsyed@ksu.edu.sa

cancer, etc., in humans [28]. For the treatment of dyes, various physicochemical and biological processes have been developed; each of them has some advantages and disadvantages [29]. The most useful and important method is semiconductor photocatalysis. It is cheap, easy to synthesize, and also has high removal efficiency of dyes [30]. Numerous metal oxides such as Fe<sub>2</sub>O<sub>3</sub>, ZnO, TiO<sub>2</sub>, and Co<sub>3</sub>O<sub>4</sub> are used as photocatalysts for dye degradation [31-33]. Zinc oxide nanoparticles (ZnO NPs) are able to remove both cationic and anionic dyes and also have good adsorption capacity, reusability, selectivity, and antibacterial properties [34]. There were two ways to modify the metal oxide nanoparticles: the first is doping with other metals, non-metals, and metal oxides; and the second method is the synthesis of the composite of metal oxides with macromolecules or polymers [35]. β-Cyclodextrin (β-CD) is a common host molecule and possesses photocatalyst, energy transfer, drug carrier, and photoelectric activities [36]. β-CD is a biodegradable oligosaccharide and its modified form is used in photocatalytic degradation [37], cell imaging [38], decolouration of ethyl violet dye [39], oil spill remediation [40], antiseptic to avoid skin diseases [41] as well as the removal of persistent organic pollutants like perfluorooctanoic acid, perfluorooctane sulphonate and Cr(VI) [42]. It is also used as a mediator between the surface of the photocatalyst and guest molecules. β-CD with metal oxide (like ZnO) composites acts as an electrondonating and hole-capturing species and enhances the photocatalytic activity via reduced charge hole recombination. β-CD used solar energy and extended up to visible light, whereas metal oxides usually used only UV rays [43].

On the other hand, nicotinic acid, also known as vitamin B3, received great attention because of its pharmaceutical use. Every year, around 20,000 tons of vitamin B3 are produced worldwide. These days, chromic acid commonly used as an oxidizing agent for the formation of vitamin B3 is characterized as corrosive. The development of an efficient catalytic system is very important to minimize the inorganic wastes and obtain vitamin B3 in high yield [44]. Owing to biological importance [45], vitamin B3 is produced by the catalytic oxidation of 3-pyridinemethanol [45], 3-pyridinecarboxyaldehyde [46], or picoline [47]. Nanostructured catalysts attract the interest of scientists because of their heterogeneous catalytic properties with improved characteristics [48,49]. Today, the use of recyclable nanocatalysts in oxidation reactions get more attention because of their eco-friendly nature [50,51].

Therefore, we described here a recyclable, eco-friendly, and efficient  $ZnO/\beta$ -CD/nicotinic acid nanocatalytic composite material, with a short reaction time. It is morphologically characterized by X-ray diffraction (XRD) and field

emission electron microscopy (FESEM). It is also characterized by UV-visible (UV-Vis) spectroscopy, band gap energy analysis, Fourier transform infrared (FTIR) spectroscopy, and weight percentage of elements determined via energy dispersive spectroscopy (EDS). We also explore the biological and photocatalytic applications of the functionalized  $\text{ZnO}/\beta\text{-CD/nicotinic}$  acid nanocomposite material.

# 2 Experimental

# 2.1 Chemical and reagents

Methylene blue (MB) and  $\beta$ -CD were obtained from Merck (99.8%). Zinc acetate dihydrate (Zn(CH<sub>3</sub>COO)<sub>2</sub>·2H<sub>2</sub>O, 99%) and other chemicals used were of analytical grade and received from Merck. Nicotinic acid and tetramethylethylenediamine (TMED) were purchased from Sigma Aldrich. All reagents and solvents were of commercial grade and used without purification. *Escherichia coli (E. coli)* and *Streptococcus aureus (S. aureus)* pure culture, agar media (Hi-Media), and PDA were used; deionized distilled water was used as a solvent.

### 2.2 Instrumentation

In the absorbance mode, UV-Vis spectra were acquired using a UV-1900i Double beam spectrophotometer. Samples were dispersed in ethanol to determine the absorbance. X-ray diffraction of the composite material was analysed using an Advanced D8 Bruker X-ray diffractometer with Ni-filtered Cu-K (1.5405) (2–10–80° and step size of 0.02°). The vibration spectra were recorded using an Avtar 370, Thermo Nicolet, Fourier transform infrared (FT-IR) spectrophotometer equipped with a DTGS detector with 4 cm<sup>-1</sup> resolution and samples were prepared with KBr discs for this study. For the FESEM study, a CARL ZEISS UHR FESEM MODEL GEMINI SEM 500 KMAT with 0.8 nm resolution and probe current of 3 pA to 100 nA was used.

### 2.3 Synthesis

### 2.3.1 Synthesis of ZnO nanoparticles

ZnO nanoparticles were synthesized by modifying the method of Royer et al. [28]. About 2.195 g of zinc acetate dihydrate was dissolved in 90 mL of ethanol under

**DE GRUYTER** 

powder.

### 2.3.2 Synthesis of the ZnO/β-CD nanocomposite material

For the synthesis of the ZnO/ $\beta$ -CD nanocomposite material, 30 mg of ZnO nanoparticles was dispersed in 10 mL of deionized water and sonicated for 15 min. After that, 30 mg of  $\beta$ -CD was dissolved in 10 mL of deionized water and stirred at 600 rpm for 10 min to obtain a transparent solution. Both solutions were mixed and continuously stirred at 600 rpm. After 6 h, the ZnO/ $\beta$ -CD nanocomposite was separated via centrifugation and washed three times with deionized water. The supernatant was freeze-dried, and the residue was weighed. Finally, the residue was dried in an oven below 80°C.

# 2.3.3 Synthesis of the ZnO/β-CD/nicotinic acid nanocomposite

For the synthesis of the ZnO/ $\beta$ -CD/nicotinic acid composite, 0.32 g of nicotinic acid was dissolved in 50 cm $^3$  of hot water (80°C) and then cooled at room temperature. Then, 0.23 g of ZnO/ $\beta$ -CD was dissolved in a 1:1 ratio of methanol/water solution. This was added to aq. solution of nicotinic acid. The reaction mixture was stirred for up to 10 min. After that, 0.39 mL of TMED was added dropwise to the reaction mixture. Then, the whole reaction mixture was stirred for up to 30 min. The resultant white crystalline material was obtained and washed with distilled water and methanol. The solid crystalline material obtained was dried under a vacuum.

# 2.4 Antibacterial activity

To determine the antibacterial activity, we used the well diffusion system on a nutrient agar medium. First, the agar medium was put into two different Petri dishes under sterile conditions and kept for 1 h for solidification. After

that, fresh, overnight-cultured *E. coli* and *S. aureus* (100  $\mu g \cdot m L^{-1}$ ) bacterial strains were spread onto both solidified agar media. Then, both the dishes were left up to 15–20 min for complete absorption of bacterial cultures. After that, three wells were prepared in each Petri dish by the gel puncture (6 mm) procedure under aseptic conditions. Samples of the ZnO/ $\beta$ -CD/nicotinic acid nanocomposite material were introduced in those wells at different concentrations of 10, 20, and 30  $\mu g \cdot m L^{-1}$ . After that, for the diffusion of the extract, both treated dishes were kept at room temperature for 30 min. Later, they were incubated at 37°C up to 24 h for maximum growth of microorganisms. After incubation, the ZnO/ $\beta$ -CD/nicotinic acid composite material showed inhibition of bacterial growth via a clear zone of inhibition (ZOI) around the well.

# 2.5 Antifungal activity

For antifungal activity, we used the well diffusion system on a PDA medium. First, the PDA medium was into a Petri dish under sterile conditions and kept for 1 h for solidification. The antifungal activity of the ZnO/β-CD/nicotinic acid nanocomposite was examined against cultured and tested fungal species Aspergillus niger (A. niger). A 5-day-old A. niger fungus was used for antifungal activity against the ZnO/β-CD/nicotinic acid nanocomposite. In this process, 3-4 mL of sterile normal saline was used for the fungal growth and gently scraped to collect the conidia. About 100 µL of the liquid spore suspension was spread evenly on the PDA dish. A sterile cork-borer was used to puncture two 6 mm-diameter circular wells on the PDA medium. Both wells of the Petri dish were filled with 20 and 40 μL of concentrated ZnO/β-CD/nicotinic acid nanocomposite to check for antifungal activity. Then, the petri dish was incubated at 25°C for 2-3 days and the zone of inhibition was measured [52].

### 2.6 Dye remediation

The MB adsorption experiment was used for photocatalysis via the ZnO/ $\beta$ -CD/nicotinic acid nanocomposite material. First, the standard stock solution of MB was made. Then, it was diluted with deionized water at various concentrations. The obtained MB solution was kept in a fixed volume flask (10 mL of 5 ppm) to which was added the ZnO/ $\beta$ -CD/nicotinic acid nanocomposite material. At room temperature, the whole solution (pH = 6) was placed in a sonicator for up to 170 min. The upper layer of the

solution was analysed at 600 nm wavelength using a UV-Vis spectrometer (UV-Visible 1900i, Shimadzu, Japan). The  $ZnO/\beta$ -CD/nicotinic acid was removed by centrifugation when the experiment was completed. The removal (R%) was calculated by Eq. 1:

$$R\% = \frac{C_0 - C_e}{C_0} \times 100$$
 (1)

where  $C_0$  is the initial concentration of MB (mg·L<sup>-1</sup>) and  $C_e$  is the equilibrium concentration of MB (mg·L<sup>-1</sup>).

# 2.7 Cytotoxicity study

The cytotoxic action of various cell lines toward different oncology products was determined using the high-throughput cell-based 3-(4,5-dimethylthiazol-2-yl)-2,5-diphenyltetrazolium bromide (MTT) assay. Cytotoxicity evaluation of the ZnO/β-CD/nicotinic acid nanocomposite was performed using MCF-7 cell lines collected from the cryopreservation cells that were thawed properly. They were initially grown in Dulbecco's modified Eagle's medium (DMEM) in a 50 mL flask with 5% fetal bovine serum and antibiotics in a 5% CO2 incubator. After incubation, the affluent cells were counted with a Neubauer chamber, and different concentrations of cells were seeded in 96 well plates. The twofold serially diluted ZnO/β-CD/nicotinic acid nanocomposite was added to the 96 well plates and incubated at 37°C for 2 h in a 5% CO2 incubator. After incubation, 96-well plates were washed and 100 µL of the MTT reagent was added to each well. After incubation for 4 h, the plates were washed with PBS buffer, and 100 µL of dimethyl sulphoxide was added to solubilize the unbounded formazan, followed by measuring the absorbance of the plate at 570 nm using a plate reader (Biotek, USA). The complete evaluation was carried out in triplicate, and it was based on the formazan dye's colour intensity, which was assumed to be directly proportional to the number of live cells.

### 3 Results and discussion

# 3.1 Characterization of nanocomposite materials

### 3.1.1 UV-Vis absorption

The UV-Vis spectra of the functionalized ZnO/ $\beta$ -CD/nicotinic acid nanocomposite material showed an absorption peak at 217 and 353 nm with one hump at 304 nm (Figure 1).

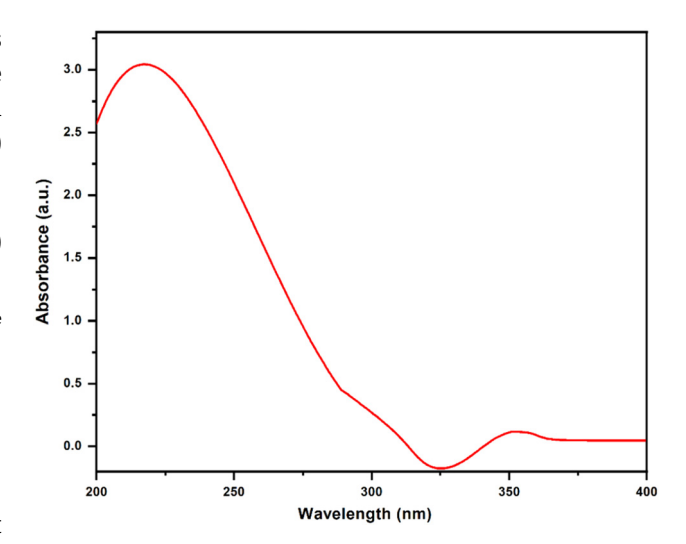


**Figure 1:** The UV-Vis absorption spectrum of the ZnO/ $\beta$ -CD/nicotinic acid nanocomposite.

The characteristic absorption spectra of the ZnO composite material in the quantum size regime absorption observed blue shift [53].

The optical bandgap ( $E_g$ ) of the nanomaterial can be determined using the classical Tauc approach [54], which shows a relationship between the incident photoenergy ( $h\nu$ ) and the absorption coefficient (a) near the absorption edge, as follows (Eq. 2):

$$\alpha h \nu = A_0 (h \nu - E_g)^n \tag{2}$$

It depends on the interband transition (e.g. n = 1/2 for direct transitions and n = 2 for indirect transitions).  $A_0$  is a constant, band tailing parameter and  $E_g$  is the intercept of the extrapolated line, when  $(\alpha h \nu)^{1/n}$  vs  $h \nu$  is plotted. Figure 2

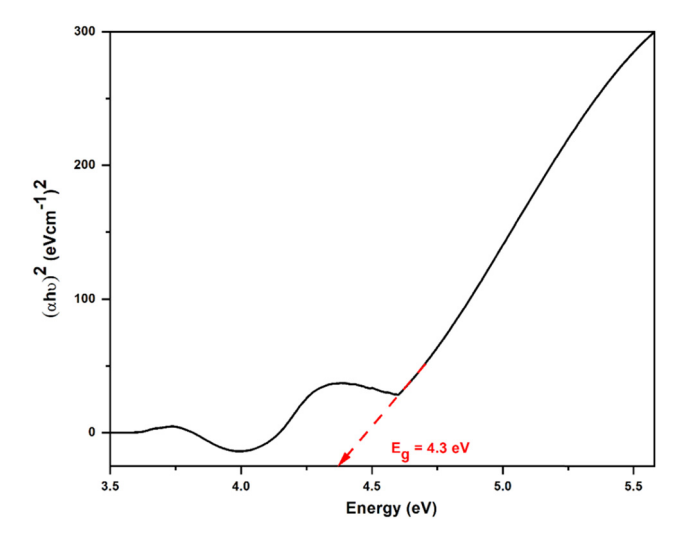


**Figure 2:** The Tauc plot of the ZnO/β-CD/nicotinic acid composite material, which was derived from UV-Vis absorption, where the band gap value ( $E_q$ ) was 4.3 eV.

shows a Tauc plot of  $ZnO/\beta$ -CD/nicotinic acid nanocomposite and the band gap value was  $4.3\,\text{eV}$ .

) FTID .......

### 3.1.2 FTIR spectra

The FTIR spectrum (Figure 3) shows that water molecules and organic moieties are present in the precursor of the nanocomposite material. The FTIR spectrum of the ZnO/β-CD/nicotinic acid nanocomposite material showed a broad peak at 3,153.38 cm<sup>-1</sup>, which is a characteristic peak of the O-H group. The H-O-H bond of β-CD has a prominent absorption peak at 1,639.09 cm<sup>-1</sup>. The peak at 1,581.78 cm<sup>-1</sup> is attributed to  $v_{as}(COO^-)$  (asymmetric stretches). The peaks at 1,472.45 and 1,426.19 cm<sup>-1</sup> are attributed to v(C=C) and v(C=N) of nicotinic acid. The peak at 1,400.53 cm<sup>-1</sup> is assigned for  $v_s(COO^-)$  (symmetric stretch) of the carboxyl group (18-009). The peaks at 1,315.09 and 1,189.85 cm<sup>-1</sup> correspond to the bending signals of the imidazole ring and C-N stretching vibrations [55,56]. The peak at 1,156.94, 1,099.05, 1,045.08, and 1,016 cm<sup>-1</sup> correspond to v(C–O), C–O–C of β-CD attached to ZnO. The peaks observed at 906.75, 816.86, 762.14, 749.76, 704.93, 995, and 760 cm<sup>-1</sup> can be assigned to C-N and C-H bending vibrations, respectively. Most characteristic peaks occur at 500-400 cm<sup>-1</sup>, which correspond to the Zn-O bond [38,57]. The Zn-O and Zn-N bonding vibration exhibited peaks at 421.31 and 571.87 cm<sup>-1</sup> for Zn–O and the Zn–N stretching mode, respectively.

#### 3.1.3 XRD

The XRD pattern of hexagonal ZnO/ $\beta$ -CD/nicotinic acid composite nanomaterials is described in Figure 4. It has a similarity with the ZnO wurtzite structure [58]. The XRD peak values relate to diffraction peaks such as  $2\theta$ , (h k l), and interplanar spacing  $d_{hkl}$  as described in Table 1. In the XRD pattern, a few peaks different, in comparison with the pure ZnO structure are observed, which indicates that the synthesized nanomaterial was the composite of ZnO/ $\beta$ -CD/nicotinic acid. With the increase in the calcination temperature, the intensity of XRD peaks and the average crystallite size increased [59]. At high temperatures, small grains aggregate to form large particles, and migration of molecules is observed.

The XRD of the  $ZnO/\beta$ -CD/nicotinic acid nanocomposites was analysed using the following formula [60]:

$$\frac{1}{d_{hkl}^2} = \frac{4}{3} \left[ \frac{h^2 + hk + k^2}{a^2} \right] + \frac{l^2}{c^2}$$
 (3)

where d is the inter-planar spacing; h, k, l are Miller indices; a and c are lattice constants with a = 3.2554 Å, c = 4.9569 Å, and c/a = 1.5227 Å.

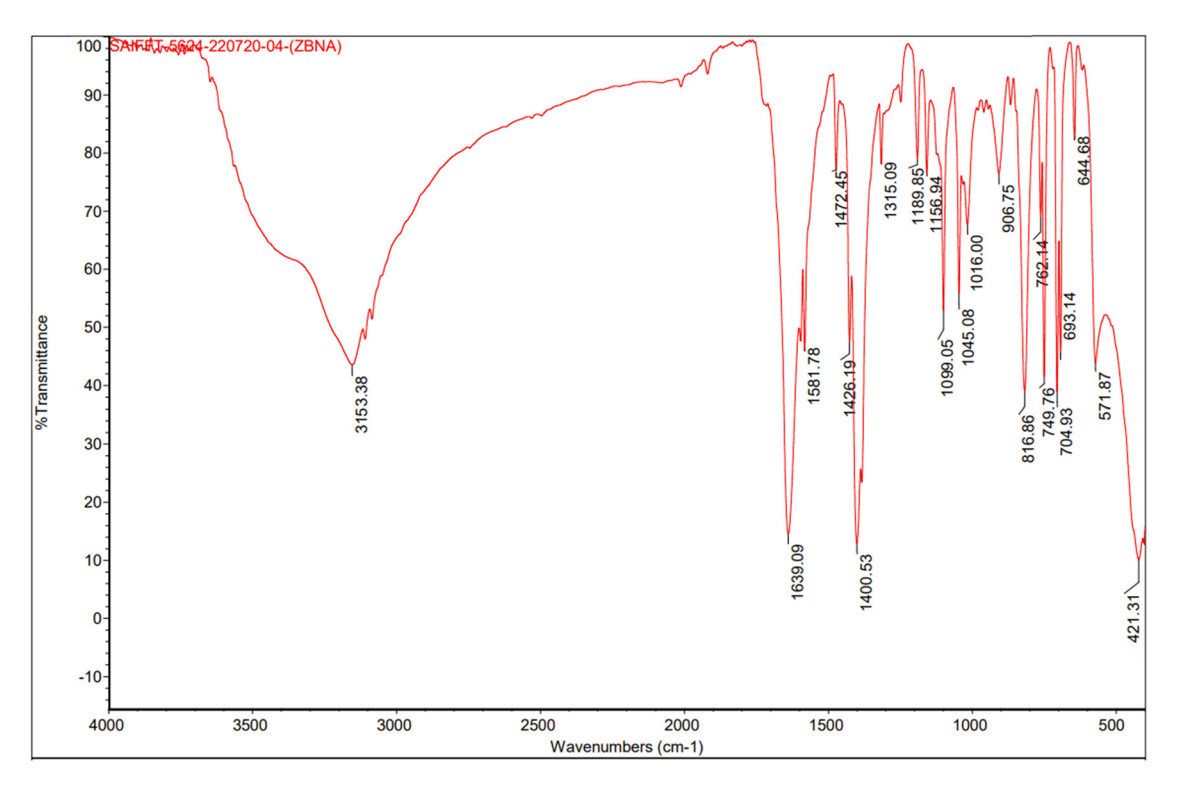
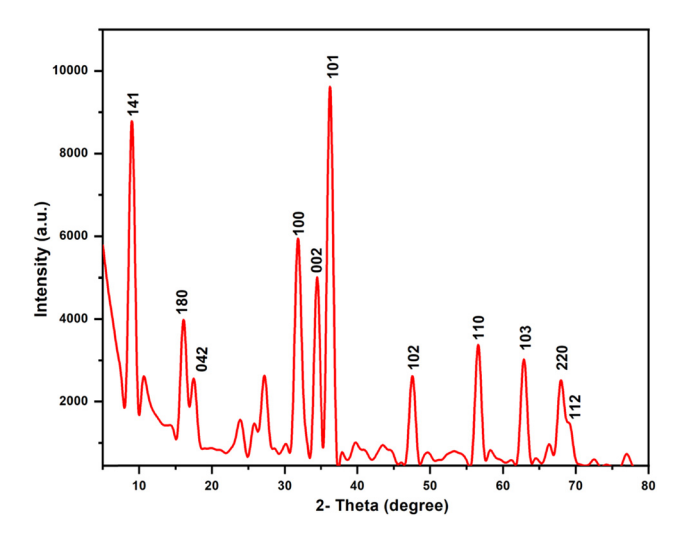


Figure 3: The FTIR spectrum of the ZnO/β-CD/nicotinic acid nanocomposite material.



**Figure 4:** The XRD spectrum of the ZnO/β-CD/nicotinic acid (ZnO/β-CD/nicotinic acid) nanocomposite material.

**Table 1:** Recycling of the used nanocatalyst ZnO/ $\beta$ -CD/nicotinic acid composite material

| SI. no. | Recycling | Time of reaction (min) | Yield after wash (%) |
|---------|-----------|------------------------|----------------------|
| 1.      | 1st       | 190                    | 95.4                 |
| 2.      | 2nd       | 190                    | 94.0                 |
| 3.      | 3rd       | 190                    | 93.1                 |
| 4.      | 4th       | 190                    | 91.7                 |
| 5.      | 5th       | 190                    | 90.0                 |

The presence of finite broadening in the XRD diffraction peaks showed that the ZnO composite material had a nanometre range. The average crystallite size of the synthesized ZnO/ $\beta$ -CD/nicotinic acid nanocomposite material was calculated using the Debye–Scherrer's formula [61] as follows:

$$D = \frac{0.9\lambda}{\beta \cos \theta} \tag{4}$$

where  $\lambda$  is the wavelength of the source Cu K $\alpha$  (0.15406);  $\beta$  is full width at half-maximum of the XRD peak; and  $\theta$  is the diffraction angle of the peak.

The crystallinity of the functionalized ZnO/ $\beta$ -CD/nicotinic acid composite material was confirmed by XRD analysis (Figure 4). The XRD pattern of the functionalized ZnO nanocomposite material exhibited peaks at  $2\theta=8.95^\circ$ ,  $16.02^\circ$ ,  $17.53^\circ$ ,  $31.74^\circ$ ,  $34.38^\circ$ ,  $36.11^\circ$ ,  $47.46^\circ$ ,  $56.57^\circ$ ,  $62.82^\circ$ ,  $67.85^\circ$ , and  $69.05^\circ$  corresponding to (141), (180), (042), (002), (101), (102), (110), (103), (220), and (112) planes of the hexagonal ZnO/ $\beta$ -CD/nicotinic acid nanocomposite, respectively (Figure 4 and Table 1). Also, we calculated the average

particle sizes using the first three prominent peaks at  $2\theta = 31.74^{\circ}$ ,  $34.38^{\circ}$ , and  $36.11^{\circ}$ , which are indexed as (100), (002), and (101) peaks of the X-ray diffraction, respectively. The grain sizes were calculated to be 45.87, 51.21, and 55.28 nm, respectively. Thus, the average size of nanoparticles was around 50 nm.

#### 3.1.4 **FESEM**

The morphological analysis of the ZnO/ $\beta$ -CD/nicotinic acid (ZnO/ $\beta$ -CD/nicotinic acid) nanocomposite material was done using FESEM (Figure 5). The FESEM images of the functionalized ZnO/ $\beta$ -CD/nicotinic acid nanocomposite material on a graphite surface are shown in Figure 5. As clearly shown in Figure 5, the ZnO nanocomposite sample was uniformly dispersed on the surface. The incorporation of functionalized ZnO composite promoted the migration of vacancies from the pores of the grain of the nanocomposite, which ultimately creates voids in the electrode. These voids provided a path for the ionic movement.

Here, the surface of the ZnO/ $\beta$ -CD/nicotinic acid nanomaterial composite was loosely packed and was hexagonal disk-shaped, which was more active. Thus, its photocatalytic activity is increased due to the aggregation of the composite on surfaces. It provided a superior adsorption environment and more active sites for the photocatalytic reaction.

### 3.1.5 EDS

The elemental composition and the purity of  $ZnO/\beta$ -CD/nicotinic acid nanocomposite material were determined

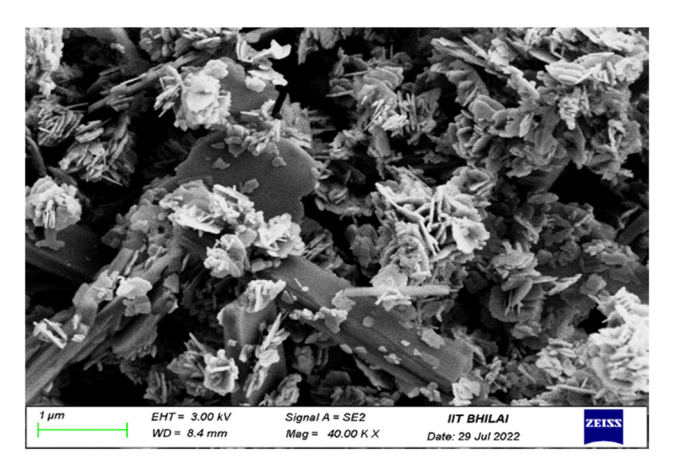
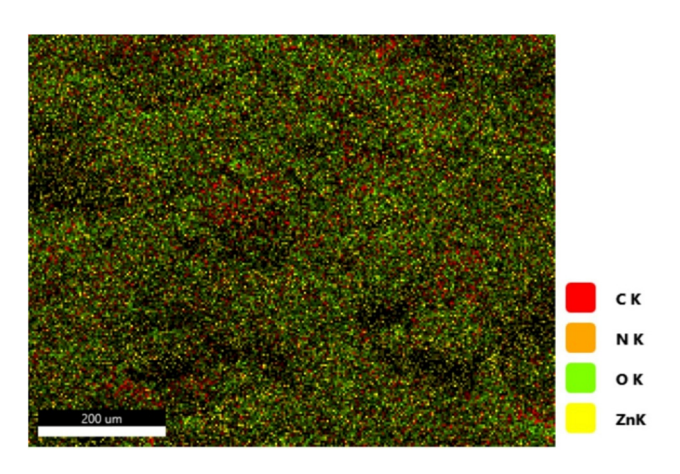


Figure 5: The FESEM image of the ZnO/ $\beta$ -CD/nicotinic acid nanocomposite material.

by EDS analysis (Figure 7). A uniform distribution of C, N, O, and Zn on the matrix was observed in the EDS spectrum and mapping (Figures 6 and 7). No other corresponding peak of impurity was observed. It contained a smooth surface, which was associated with heterogenous mixing of C, N, O, and Zn, resulting in a single-phase surface morphology as observed (Figure 7).

# 3.2 Photocatalysis

The photocatalytic experiment of  $ZnO/\beta$ -CD/nicotinic acid nanocomposite samples was analysed via the degradation of MB dye in aqueous solution under UV and visible irradiation. The photodegradation experiment was followed



**Figure 6:** EDS mapping for the ZnO/ $\beta$ -CD/nicotinic acid nanocomposite material.

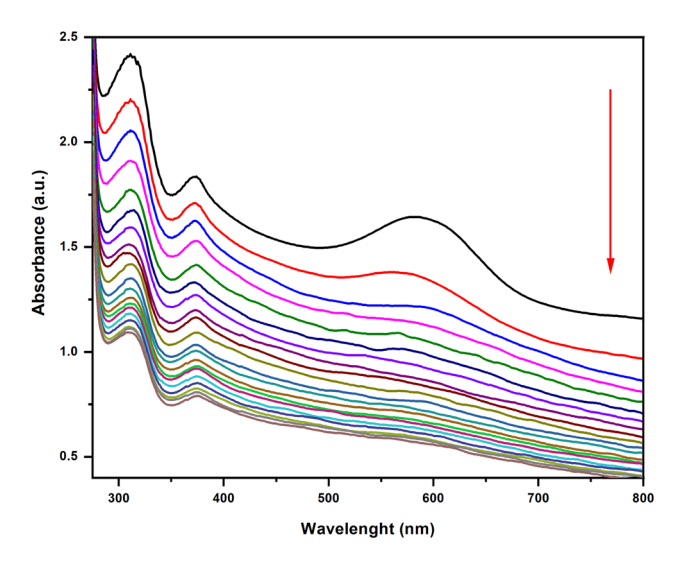


**Figure 8:** The photocatalysis experiment via the absorption spectra of MB dye with the ZnO/β-CD/nicotinic acid nanocomposite material under UV-Vis irradiation.

by UV-Vis absorption spectroscopy at different irradiation times (Figure 8) [62].

In this photocatalysis process, the MB dye was degraded under light irradiation, where UV-Vis light was used as an irradiation source. We described here the photocatalysis reaction of ZnO/ $\beta$ -CD/nicotinic acid nanocomposite with MB. In the presence of light and air, 40.0 mg of the ZnO/ $\beta$ -CD/nicotinic acid nanocomposite material was added to 10.0 mL aq. solution of MB (1.0 × 10<sup>-4</sup> M) (pH = 6). After 10 min, the degradation of blue colour starts. At a constant time (10 min) interval, the ZnO/ $\beta$ -CD/nicotinic acid nanocomposite degrades the blue colour of the solution (Figure 8).

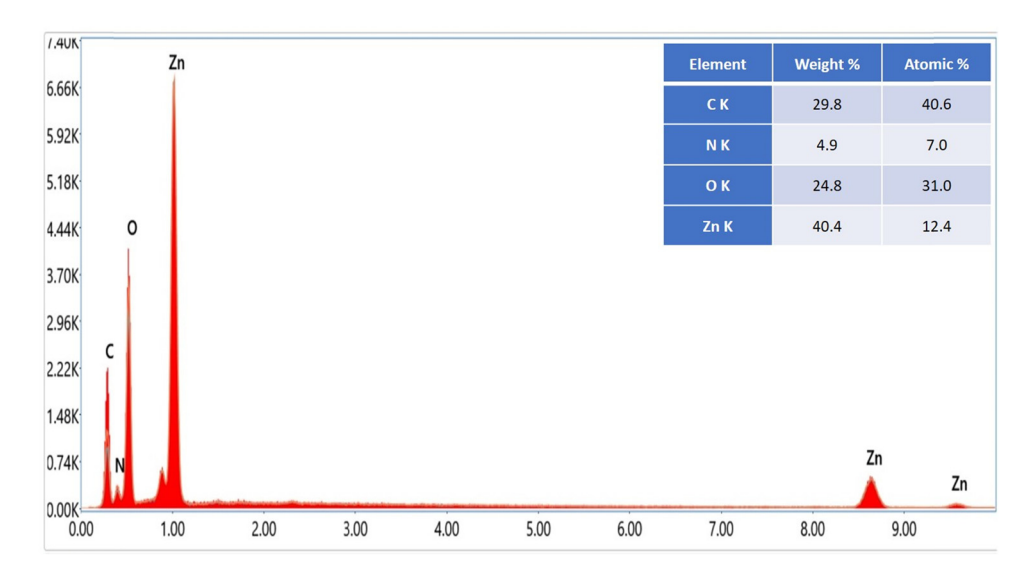
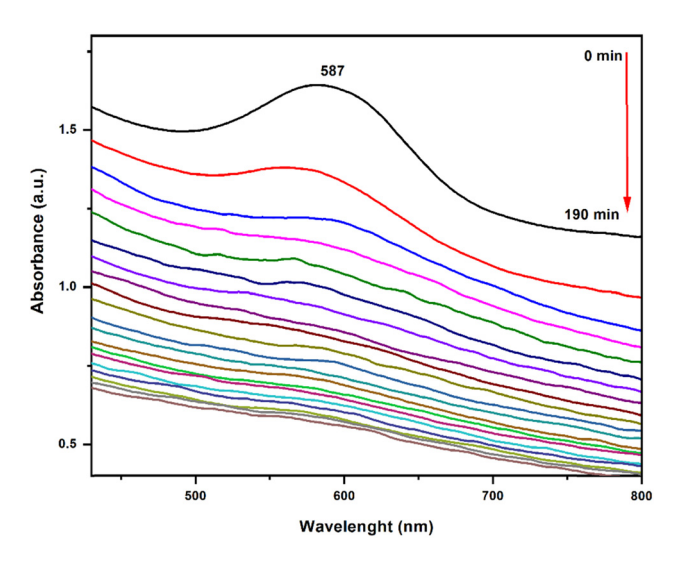


Figure 7: The EDS spectrum with a weight percentage table of ZnO-β-CD.

A scanning range between 200 and 800 nm was used for the MB solution. According to previous studies, the absorption peak of MB was observed at 650 nm. After adding 40.0 mg of the ZnO/ $\beta$ -CD/nicotinic acid nanocomposite, the absorption peak shifted and  $\lambda_{\rm max}$  was obtained at 587 nm because of the formation of tetramer, which is responsible for the blue shift [63].

In the presence of visible light, the  $ZnO/\beta$ -CD/nicotinic acid nanocomposite material formed  $OH^-$  in the presence of water ( $H_2O$ ). The whole reaction was monitored via MB



**Figure 9:** Demonstration of the photodegradation process of MB in the presence of ZnO/ $\beta$ -CD/nicotinic acid nanocomposite at a 587 nm wavelength up to 190 min.

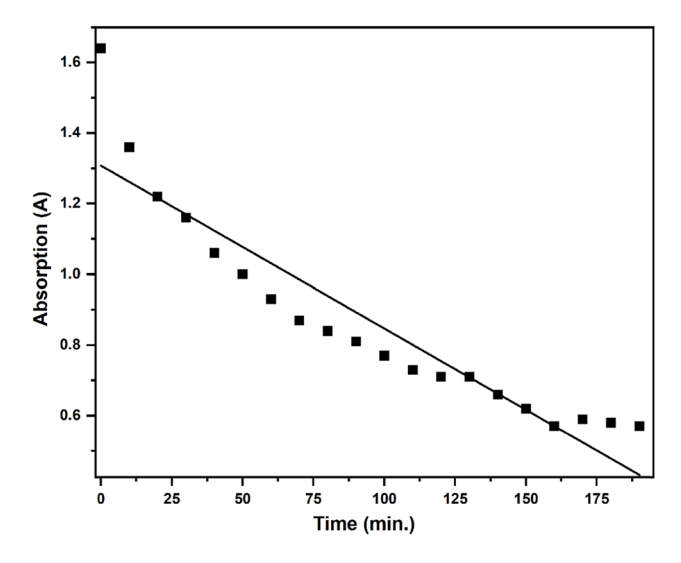


**Figure 10:** The addition of the ZnO/ $\beta$ -CD/nicotinic acid nanocomposite material (40.0 mg), at 587 nm wavelength. The time increased, the absorption decreased up to 190 min at a constant time interval (10 min) and the blue colour of the solution was decolourized.

degradation at 587 nm wavelength in an aq. solution by a decrease in the absorbance (Figure 9).

According to Figure 9, in the presence of the ZnO/ $\beta$ -CD/nicotinic acid nanocomposite, the blue colour of aq. MB dye decreased with time, and it was clearly observed at a wavelength of 587 nm. At a constant time interval (10 min), the blue colour decreased and the peak at 587 nm also decreased. After 190 min, the peak converted into a straight line and the blue colour of the aq. solution of MB became transparent and colourless.

According to Figure 10, at 587 nm wavelength, the absorption decreased at a constant time interval (10 min). After 10 min, the absorption was decreased and as time increased, the absorption of blue dye decreased. Resultant force of optical density, get a straight line with constant time interval (10 min). After the completion of the photodegradation process, the absorption was constant and the blue colour of the solution also turned colourless.

# 3.3 Cytotoxicity test (MTT assay)

The MTT assay is a high-throughput cell-based assay and is used to evaluate the cytotoxic response of different cell lines to different oncology products. In the present work, the MTT assay was reformed as a chemosensitivity test and its potential was examined. This technique also has numerous benefits regarding speed, quantitation, managing various samples, and cell number. The application of this assay for chemosensitivity testing appears to be valuable and advantageous. MTT examines cell respiration, and the amount of formazan formed is proportional to the number of living cells present in the culture. An increase or reduction in the cell number results in a concomitant change in the quantity of formazan formed, demonstrating the degree of cytotoxicity initiated by the drug. The IC<sub>50</sub> (concentration) value of the tested drug determines the ability of the drug to cause the death of 50% of the cells and can predict the degree of its cytotoxic effect. The lower the value, the more cytotoxic the substance will be. Figure 11 shows the comparative graph of the IC<sub>50</sub> values of as-synthesized ZnO/β-CD/nicotinic acid nanocomposites against MCF-7 cancer cell lines. The percentage cell viability of cancer cells response to various doses of ZnO/β-CD/nicotinic acid nanocomposite is shown. The ZnO/β-CD/nicotinic acid nanocomposite ability to promote cell proliferation was tested at concentrations between 0.7 and  $200 \,\mu \text{g} \cdot \text{mL}^{-1}$ ; the IC<sub>50</sub> value was  $14.95 \,\mu \text{g} \cdot \text{mL}^{-1}$  after 24 h. The cytotoxicity results clearly indicate that the ZnO/β-CD/nicotinic acid nanocomposite has the best ability to be used as an anticancer agent in oncology

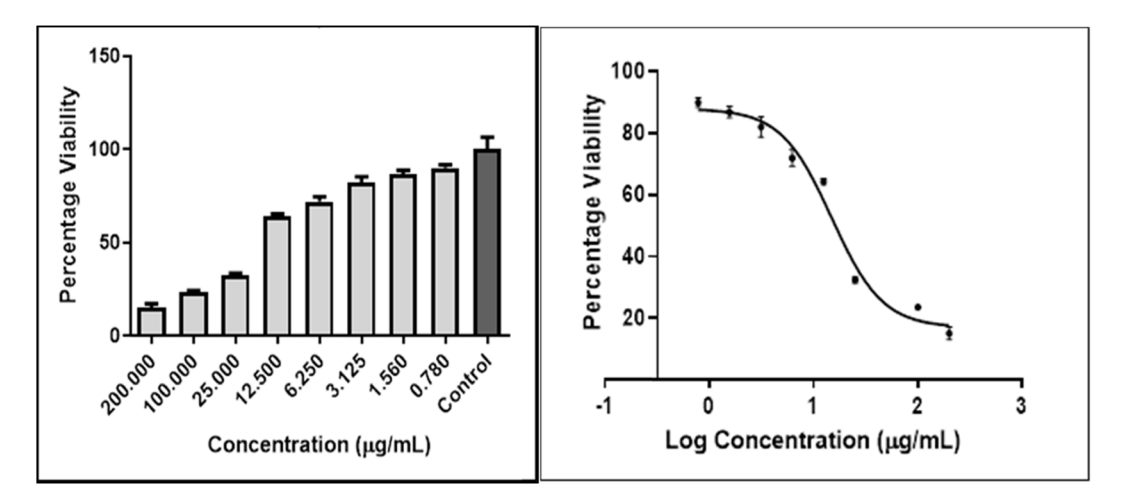


**Figure 11:** The MTT assay using the ZnO/β-CD/nicotinic acid nanocomposite in MCF-7 cell lines.

treatment. ZnO nanoparticles are known to be a potential anticancer agent, which was proven by many previous studies [64].

# 3.4 Reuse of the catalyst

For the reuse of the catalyst, the stability of the catalyst is highly important. We use the Fenton reaction to evaluate the stability of the  $\text{ZnO}/\beta\text{-CD}/\text{nicotinic}$  acid nanocomposite material; we used it many times for several consecutive MB removal cycles. At each cycle, the solid nanocomposite catalyst was separated by centrifugation from the solution and washed with ethanol and distilled water. After that, it was dried in a vacuum and was ready to be reused as a catalyst in the next reaction. In the whole process, we also

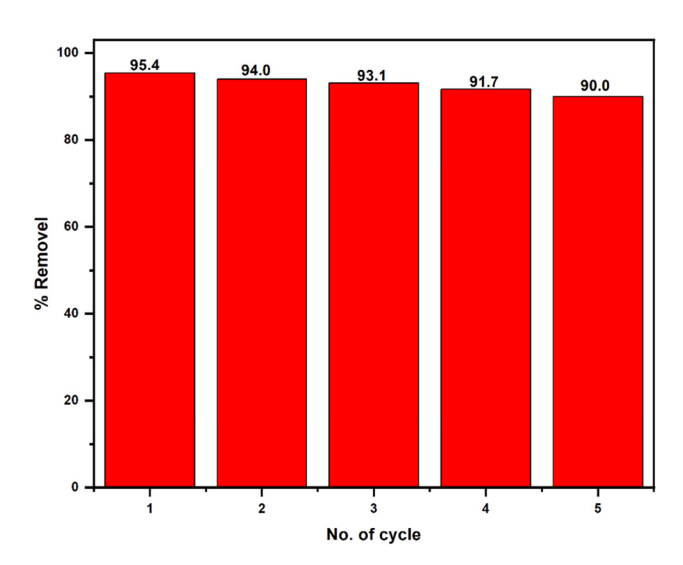


**Figure 12:** Recycling experiment of ZnO/ $\beta$ -CD/nicotinic acid nanocomposite materials for the MB degradation process.

observed a slight weight loss of the catalyst after every cycle (190 min). As shown in Figure 12, it is clear that the weight of ZnO/ $\beta$ -CD/nicotinic acid nanocomposite material decreased in each cycle from 95.4%, 94.0%, 93.1%, and 91.7%, and retained up to 90.0% of its catalytic activity after 5th cycle (Table 1). The small decrease in its catalytic activity after each cycle might be attributed to its incomplete removal during washing. This showed that the ZnO/ $\beta$ -CD/nicotinic acid nanocomposite was highly stable in an aqueous solution during the photocatalysis process.

### 3.5 Antimicrobial activity

The antibacterial properties of the ZnO- $\beta$ -CD nanocomposite material prevented further growth of two bacterial strains *E. coli* and *S. aureus*. Figure 13 shows that the different ZOI (zones of inhibition) for antibacterial activity obtained with different concentrations (10, 50, and 100 µg·mL $^{-1}$ ) of the ZnO/ $\beta$ -CD/nicotinic acid (ZnO/ $\beta$ -CD/nicotinic acid) nanocomposite. It is clear that the ZnO/ $\beta$ -CD/nicotinic acid (ZnO/ $\beta$ -CD/nicotinic acid) nanocomposite produced a good ZOI for the *S. aureus* bacterial strain (Figure 13a) with a clear area around the sample showing complete inhibition. But with *E. coli* it did not show the ZOI area (Figure 13b). The probable antimicrobial action of the nanocomposite is due to the inhibition of microbial proteins causing eventual cell damage and the death of microbes [65].

The antifungal activity was studied with different concentrations (20 and 40  $\mu$ L) of the ZnO/ $\beta$ -CD/nicotinic acid (ZnO/ $\beta$ -CD/nicotinic acid) nanocomposite. It clearly showed that ZnO/ $\beta$ -CD/nicotinic acid (ZnO/ $\beta$ -CD/nicotinic acid) produced a minimum ZOI for *A. niger* (Figure 14b). The clear area around the sample showed a complete inhibition

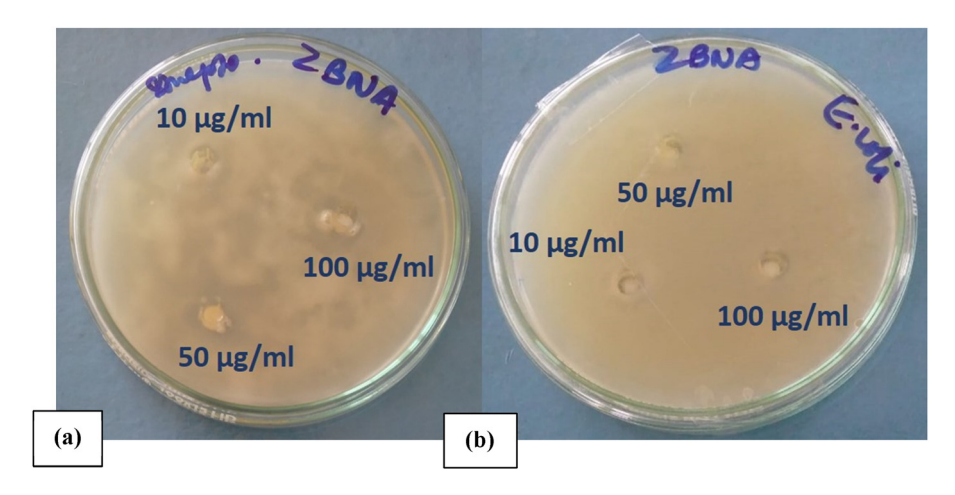
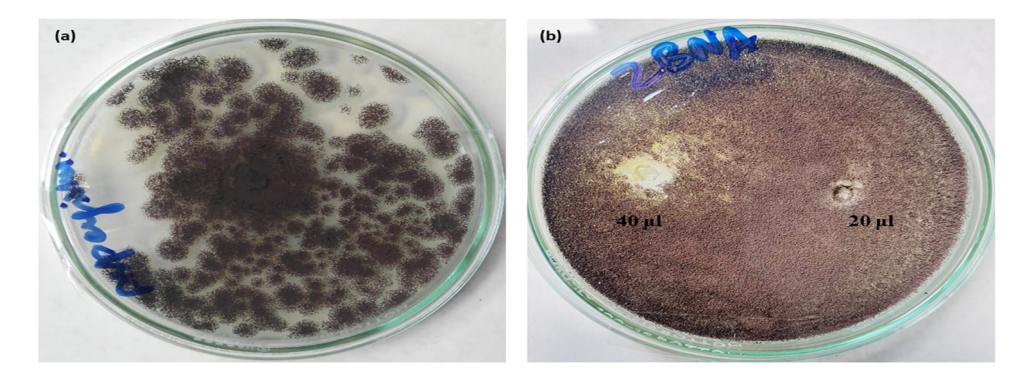


Figure 13: (a) *S. aureus*- and (b) *E. coli*-treated with the ZnO/β-CD/nicotinic acid nanocomposite material at different concentrations in methanol (10, 50, and 100  $\mu$ g·mL<sup>-1</sup>).



**Figure 14:** (a) The colony of cultured *Aspergillus niger* fungal strain; (b) *Aspergillus niger*-treated with the ZnO/β-CD/nicotinic acid nanocomposite material at different concentrations in methanol (20 and 40 μL).

zone. Figure 14 shows that increased concentrations of the ZnO/ $\beta$ -CD/nicotinic acid nanocomposite result in the decreased growth rate of *Aspergillus niger*. On comparison of both wells, the well with 40  $\mu$ L of the ZnO composite sample showed good activity than the well with 20  $\mu$ L of the sample. When *A. niger* was treated with the Zn/ $\beta$ -CD/nicotinic acid nanocomposite, it released proteins, carbohydrates, and lipids by damaging the cell membranes. As a result, decreased amounts of proteins, carbohydrates, and lipids were observed in the fungal cells, which leads to the death of the cells [66,67].

# 3.6 Photocatalytic degradation mechanism

The photocatalysis mechanisms are described via the photodegradation of MB by the ZnO/ $\beta$ -CD/nicotinic acid nanocomposite material in the presence of UV-Vis light and air [59,68–73]. It can be explained as follows: In the photocatalysis process at a 587 nm wavelength,  $1.0 \times 10^{-4}$  M

MB dye was mixed with 40.0 mg of the ZnO/β-CD/nicotinic acid nanocomposite material. The solution mixture of MB and the ZnO/β-CD/nicotinic acid nanocomposite vessel was photo-irradiated under UV/visible light; the ZnO composite is excited. Due to the excitation of the composite material, photo-induced pairs of electrons and holes (e<sup>-</sup> + h<sup>+</sup>) are formed. These electrons or holes are captured by the aqueous solution of MB dye and radicals like OH and O<sub>2</sub> are generated, which decolourized the blue colour of MB [73,74]. The active sites of the ZnO composite catalyst are covered by the MB dye and degradation products, which compete with the H<sub>2</sub>O and OH to be adsorbed on the same sites; as a result fewer OH' radicals are formed and high degradation efficiency is observed [75]. A specific amount of light radiation is used by the MB dye molecules and less amount of photons reach the surface of the catalyst to generate OH radicals [74,76].

The MB dye enters into the holes of the  $ZnO/\beta$ -CD/nicotinic acid composite (which binds with ZnO centrally) surface and absorbs radiation of light for excitation. An electron rapidly

excites the MB dye to the conduction band of ZnO. Along with the OH radical, another important radical, the superoxide anion radical ( $O_2^-$ ), is illuminated from the ZnO nanocomposite. Thus, the excited MB dye with the ZnO/ $\beta$ -CD/nicotinic acid composite material undergoes the photocatalytic degradation reaction [77,78]. The mechanism reaction is as follows:

ZnO/β-CD/nicotinic acid + 
$$hv$$
  
 $\rightarrow$  ZnO/β-CD/nicotinic acid +  $e^-$  +  $h^+$  (5)

$$e^- + O_2 \rightarrow \cdot O_2^-$$
 (6)

$$h^+ + H_2O \rightarrow 'OH^-$$
 (7)

$$MB + OH \rightarrow de$$
-colourized blue colour (8)

$$MB + O_2^- \rightarrow de$$
-colourized blue colour (9)

In summary, in the presence of light and air, the ZnO/β-CD/nicotinic acid nanocomposite material generates holes and electrons. They react with water and form 'O<sub>2</sub> and 'OH<sup>-</sup> radicals, which are used in the photocatalysis or in the photodegradation process of MB at pH 6 of the solution. In an acidic medium, the rate of degradation was high in comparison with the basic medium because the negatively charged hydroxyl radicals easily degrade the cationic dye. At a constant time interval, the activity of the ZnO/β-CD/nicotinic acid nanocomposite material decreases because of the formation of a layer of OH that coats the surface of the catalyst, which could be washed with ethanol and distilled water. After drying the solid nanocomposite, it can again be reused for the next catalysis reaction cycle. After each cycle, the activity of the catalyst for degradation is slightly decreased and after the 5th cycle, it would be around 90%. These ZnO/β-CD/nicotinic acid nanocomposites are also used as antibacterial or growth inhibitors against E. coli and S. aureus bacterial strains. At high optical density, the nanocomposites damaged the cell membranes of S. aureus. As a result, at high optical density, colony growth was not observed; for E. coli it did not show any result. The ZnO/β-CD/nicotinic acid nanocomposite produced a clear ZOI for S. aureus but for E. coli, no clear region was observed around the wells. Similar to antibacterial activity, the Zn/β-CD/nicotinic acid nanocomposite showed antifungal activity for the A. niger fungal strain.

## 4 Conclusion

Here, we synthesized  $ZnO/\beta$ -CD/nicotinic acid nanocomposites using the co-precipitation method with aq. solvent. The reaction between both precursors in the presence of water generated  $OH^-$  ions for precipitation. The

synthesized ZnO/β-CD/nicotinic acid nanocomposite was characterized, and the average XRD crystallite size was 50 nm as calculated using the Scherrer formula. It also showed a remarkable photocatalytic property with MB. The ZnO/β-CD/nicotinic acid composite showed good catalytic efficiency in the degradation of MB at pH 6 in comparison with ZnO. The blue colour of MB was decolourized at a constant time interval. After 190 min, the blue colour of the solution became colourless. This process provided easy recovery of the nanocomposite catalyst by centrifugation and separation. The catalytic activity was again regained in consecutive steps. The degradation efficiency was around 90%. Due to the generation of 'O<sub>2</sub><sup>-</sup> and 'OH<sup>-</sup> radicals by the ZnO/β-CD/nicotinic acid nanocomposite material, it was also used as antibacterial or growth inhibitors against S. aureus bacterial strains, but it did not show any antibacterial effect against E. coli. It was also used as an antifungal growth inhibitor for A. niger fungal strains. The prepared materials also showed the efficacy of anticancer activity towards MCF-7 cell lines.

**Acknowledgements:** The authors extend their appreciation to the Researchers Supporting Project number (RSPD 2023R739), King Saud University, Riyadh, Saudi Arabia for funding this work.

**Funding information:** This research was funded by the Researchers Supporting Project number (RSPD2023R739), King Saud University, Riyadh, Saudi Arabia.

**Author contributions:** Mohammed S. Alqahtani and Rabbani Syed: writing – original draft, writing – review and editing, methodology, formal analysis; Mudassar Shahid and Jilani Purusottapatnam Shaik: writing – original draft, formal analysis, visualization, project administration; Rabbani Syed: funding and resources.

Conflict of interest: The authors state no conflict of interest.

**Data availability statement:** All the data are available in the manuscript.

# References

- Khan I, Saeed K, Khan I. Nanoparticles: Properties, applications and toxicities. Arab J Chem. 2019;12(7):908–31.
- [2] Chakraborty B, Indra A, Menezes PV, Drieß M, Menezes PW. Improved chemical water oxidation with Zn in the tetrahedral site of spinel-type ZnCo2O4 nanostructure. Mater Today Chem. 2020;15:100226.

- Devasangeeth SD, Balaji GL, Lakshmipathy R. Synthesis of surfacefunctionalized ZnS nanoparticles and its potential application as methylene blue adsorbent. Desalination Water Treat. 2018;108:353-61.
- [4] Lakshmipathy R, Kesarla MK, Nimmala AR, Godavarthi S, Kukkambakam CM, Gomez LM, et al. ZnS nanoparticles capped with watermelon rind extract and their potential application in dye degradation, Res Chem Intermed, 2017:43:1329-39.
- Berube DM. Rhetorical gamesmanship in the nano debates over sunscreens and nanoparticles. J Nanopart Res. 2008;10:23-37.
- Brida D, Fortunato E, Águas H, Silva V, Marques A, Pereira L, et al. New insights on large area flexible position sensitive detectors. J Non-Cryst Solids. 2002;299:1272-6.
- Tripathi M. Kumar A. Zinc oxide nanofiller-based composite polymer gel electrolyte for application in EDLCs. Ionics. 2018;24(10):3155-65.
- Suchea M, Christoulakis S, Moschovis K, Katsarakis N, Kiriakidis G. ZnO transparent thin films for gas sensor applications. Thin Solid films. 2006;515(2):551-4.
- Ashour A, Kaid MA, El-Sayed NZ, Ibrahim AA. Physical properties of ZnO thin films deposited by spray pyrolysis technique. Appl Surf Sci. 2006;252(22):7844-8.
- [10] Seiyama T, Kato A, Fujiishi K, Nagatani M. A new detector for gaseous components using semiconductive thin films. Anal Chem. 1962;34(11):1502-3.
- Yamazoe N, Sakai G, Shimanoe K. Oxide semiconductor gas sensors. Catal Surv Asia. 2003;7:63-75.
- [12] Uekawa N, Yamashita R, Wu YJ, Kakegawa K. Effect of alkali metal hydroxide on formation processes of zinc oxide crystallites from aqueous solutions containing Zn(OH)<sup>2</sup> ions. Phys Chem Chem Phys. 2004;6(2):442-6.
- [13] Mo M, Yu JC, Zhang L, Li SK. Self-assembly of ZnO nanorods and nanosheets into hollow microhemispheres and microspheres. Adv Mater. 2005;17(6):756-60.
- [14] Lao JY, Wen JG, Ren ZF. Hierarchical ZnO nanostructures. Nano Lett. 2002:2(11):1287-91.
- [15] Gao PX, Wang ZL. Mesoporous polyhedral cages and shells formed by textured self-assembly of ZnO nanocrystals. J Am Chem Soc. 2003;125(37):11299-305.
- [16] Zhang H, Yang D, Ji Y, Ma X, Xu J, Que D. Low temperature synthesis of flowerlike ZnO nanostructures by cetyltrimethylammonium bromide-assisted hydrothermal process. J Phys Chem B. 2004;108(13):3955-8.
- [17] Mondelaers D, Vanhoyland G, Van den Rul H, D'haen J, Van Bael MK, Mullens J, et al. Synthesis of ZnO nanopowder via an aqueous acetate-citrate gelation method. Mater Res Bull. 2002;37(5):901-14.
- [18] Tokumoto MS, Pulcinelli SH, Santilli CV, Briois V. Catalysis and temperature dependence on the formation of ZnO nanoparticles and of zinc acetate derivatives prepared by the sol - gel route. J Phys Chem B. 2003;107(2):568-74.
- [19] Singhai M, Chhabra V, Kang P, Shah DO. Synthesis of ZnO nanoparticles for varistor application using Zn-substituted aerosol OT microemulsion. Mater Res Bull. 1997;32(2):239-47.
- [20] Tsuzuki T, McCormick PG. ZnO nanoparticles synthesised by mechanochemical processing. Scr Mater. 2001;44(8-9):1731-4.
- [21] Okuyama K, Lenggoro IW. Preparation of nanoparticles via spray route. Chem Eng Sci. 2003;58(3-6):537-47.
- [22] Sato T, Tanigaki T, Suzuki H, Saito Y, Kido O, Kimura Y, Kaito C, Takeda A, Kaneko S. Structure and optical spectrum of ZnO

- nanoparticles produced in RF plasma. J Cryst Growth. 2003;255(3-4):313-6.
- [23] Liu B, Zeng HC. Hydrothermal synthesis of ZnO nanorods in the diameter regime of 50 nm. J Am Chem Soc. 2003;125(15):4430-1.
- [24] Hu XL, Zhu YJ, Wang SW. Sonochemical and microwave-assisted synthesis of linked single-crystalline ZnO rods. Mater Chem Phys. 2004;88(2-3):421-6.
- [25] Hong R, Pan T, Qian J, Li H. Synthesis and surface modification of ZnO nanoparticles. Chem Eng J. 2006;119(2-3):71-81.
- [26] Wang J, Gao L. Synthesis and characterization of ZnO nanoparticles assembled in one-dimensional order. Inorg Chem Commun. 2003;6(7):877-81.
- [27] Qiu R, Zhang D, Mo Y, Song L, Brewer E, Huang X, et al. Photocatalytic activity of polymer-modified ZnO under visible light irradiation. | Hazard Mater. 2008;156(1-3):80-5.
- [28] Royer B, Cardoso NF, Lima EC, Macedo TR, Airoldi C. A useful organofunctionalized layered silicate for textile dye removal. I Hazard Mater. 2010;181(1-3):366-74.
- [29] Lefebvre O, Moletta R. Treatment of organic pollution in industrial saline wastewater: a literature review. Water Res. 2006;40(20):3671-82.
- [30] Hu G, Zhou Z, Guo Y, Hou H, Shao S. Electrospun rhodium nanoparticle-loaded carbon nanofibers for highly selective amperometric sensing of hydrazine. Electrochem Commun. 2010;12(3):422-6.
- [31] Zhang X, Wu F, Deng N. Degradation of paracetamol in self assembly  $\beta$ -cyclodextrin/TiO2 suspension under visible irradiation. Catal Commun. 2010;11(5):422-5.
- [32] Meena S, Vaya D, Das BK. Photocatalytic degradation of Malachite Green dye by modified ZnO nanomaterial. Bull Mater Sci. 2016;39:1735-43.
- [33] Zhou X, Yang H, Wang C, Mao X, Wang Y, Yang Y, et al. Visible light induced photocatalytic degradation of rhodamine B on onedimensional iron oxide particles. J Phys Chem C. 2010;114(40):17051-61.
- [34] Rakshit S, Vasudevan S. Resonance energy transfer from β-cyclodextrin-capped ZnO: MgO nanocrystals to included Nile Red guest molecules in aqueous media. ACS Nano. 2008;2(7):1473-9.
- [35] Da Dalt S, Alves AK, Bergmann CP. Photocatalytic degradation of methyl orange dye in water solutions in the presence of MWCNT/ TiO2 composites. Mater Res Bull. 2013 May 1;48(5):1845-50.
- [36] Yan Y, Zheng Z, Deng C, Zhang X, Yang P. Facile synthesis of Ti 4 + -immobilized Fe 3 O 4@ polydopamine core-shell microspheres for highly selective enrichment of phosphopeptides. Chem Commun. 2013;49(44):5055-7.
- [37] Khammar S, Bahramifar N, Younesi H. Preparation and surface engineering of CM-β-CD functionalized Fe3O4@ TiO2 nanoparticles for photocatalytic degradation of polychlorinated biphenyls (PCBs) from transformer oil. J Hazard Mater. 2020;394:122422.
- [38] Sawant VJ, Bamane SR. PEG-beta-cyclodextrin functionalized zinc oxide nanoparticles show cell imaging with high drug payload and sustained pH responsive delivery of curcumin in to MCF-7 cells. J Drug Delivery Sci Technol. 2018;43:397-408.
- [39] Velusamy P, Pitchaimuthu S, Rajalakshmi S, Kannan N. Modification of the photocatalytic activity of TiO2 by β-Cyclodextrin in decoloration of ethyl violet dye. J Adv Res. 2014;5(1):19-25.
- [40] Kumar A, Sharma G, Naushad M, Thakur S. SPION/B-cyclodextrin core-shell nanostructures for oil spill remediation and organic pollutant removal from waste water. Chem Eng J. 2015;280:175-87.

[41] Hu JL, Lu J. Memory polymer coatings for smart textiles. In:Active Coatings for Smart Textiles. United Kingdom: Woodhead Publishing; 2016 Apr 6. p. 11-34.

**DE GRUYTER** 

- [42] Zhao Q, Zhao X, Cao J. Advanced nanomaterials for degrading persistent organic pollutants. In: Advanced Nanomaterials for Pollutant Sensing and Environmental Catalysis. Amsterdam: Elsevier; 2020. p. 249-305.
- [43] Vikrant K, Kim KH, Ok YS, Tsang DC, Tsang YF, Giri BS, et al. Engineered/designer biochar for the removal of phosphate in water and wastewater. Sci Total Environ. 2018;616:1242-60.
- [44] Raja R, Thomas JM, Greenhill-Hooper M, Ley SV, Almeida, Paz FA. Facile, one-step production of niacin (Vitamin B3) and other nitrogen-containing pharmaceutical chemicals with a single-site heterogeneous catalyst. Chem - Eur I. 2008:14(8):2340-8.
- [45] Alfè M, Spasiano D, Gargiulo V, Vitiello G, Di Capua R, Marotta R. TiO2/graphene-like photocatalysts for selective oxidation of 3pyridine-methanol to vitamin B3 under UV/solar simulated radiation in aqueous solution at room conditions: The effect of morphology on catalyst performances. Appl Catal A: Gen. 2014;487:91-9.
- [46] Yurdakal S, Yanar ŞÖ, Çetinkaya S, Alagöz O, Yalçın P, Özcan L. Green photocatalytic synthesis of vitamin B3 by Pt loaded TiO2 photocatalysts. Appl Catal B: Environ. 2017;202:500-8.
- [47] Adams RD, Chen M, Elpitiya G, Potter ME, Raja R. Iridium-bismuth cluster complexes yield bimetallic nano-catalysts for the direct oxidation of 3-picoline to niacin. ACS Catal. 2013 Dec 6;3(12):3106-10.
- [48] Polshettiwar V, Luque R, Fihri A, Zhu H, Bouhrara M, Basset JM. Magnetically recoverable nanocatalysts. Chem Rev. 2011;111(5):3036-75.
- [49] Moussa H, Girot E, Mozet K, Alem H, Medjahdi G, Schneider R. ZnO rods/reduced graphene oxide composites prepared via a solvothermal reaction for efficient sunlight-driven photocatalysis. Appl Catal B: Environ. 2016;185:11-21.
- [50] Tian J, Liu S, Li H, Wang L, Zhang Y, Luo Y, et al. One-step preparation of ZnO nanoparticle-decorated reduced graphene oxide composites and their application to photocurrent generation. RSC Adv. 2012;2(4):1318-21.
- [51] Gawande MB, Rathi AK, Tucek J, Safarova K, Bundaleski N, Teodoro OM, et al. Magnetic gold nanocatalyst (nanocat-Fe-Au): catalytic applications for the oxidative esterification and hydrogen transfer reactions. Green Chem. 2014;16(9):4137-43.
- [52] Hasnidawani JN, Azlina HN, Norita H, Bonnia NN, Ratim S, Ali ES. Synthesis of ZnO nanostructures using sol-gel method. Proc Chem. 2016;19:211-6.
- [53] Perez C. Antibiotic assay by agar-well diffusion method. Acta Biol Med Exp. 1990;15:113-5.
- [54] Singh K, Chaudhary GR, Singh S, Mehta SK. Synthesis of highly luminescent water stable ZnO quantum dots as photoluminescent sensor for picric acid. J Lumin. 2014;154:148-54.
- [55] Tauc J, editor. Amorphous and liquid semiconductors. New York: Springer Science & Business Media; 2012 Dec 6.
- [56] Khaletskaya K, Turner S, Tu M, Wannapaiboon S, Schneemann A, Meyer R, et al. Self-directed localization of ZIF-8 thin film formation by conversion of ZnO nanolayers. Adv Funct Mater. 2014;24(30):4804-11.
- [57] Do Nascimento AL, Caires FJ, Gomes DJ, Gigante AC, Ionashiro M. Thermal behaviour of nicotinic acid, sodium nicotinate and its

- compounds with some bivalent transition metal ions. Thermochim Acta. 2014:575:212-8.
- [58] Zhou W, Wu YP, Zhao J, Dong WW, Qiao XQ, Hou DF, et al. Efficient gas-sensing for formaldehyde with 3D hierarchical Co3O4 derived from Co5-based MOF microcrystals. Inorg Chem. 2017 Nov 20;56(22):14111-7.
- [59] Yadav R, Chundawat TS, Rawat P, Rao GK, Vaya D. Photocatalytic degradation of malachite green dye by ZnO and ZnO-β-cyclodextrin nanocomposite. Bull Mater Sci. 2021;44:1-8.
- [60] Kumar SS, Venkateswarlu P, Rao VR, Rao GN. Synthesis, characterization and optical properties of zinc oxide nanoparticles. Int Nano Lett. 2013;3:1-6.
- [61] Bindu P, Thomas S. Estimation of lattice strain in ZnO nanoparticles: X-ray peak profile analysis. J Theor Appl Phys. 2014;8:123-34.
- [62] De Carvalho CN, Lavareda G, Amaral A, Conde O, Ramos AR. InOx semiconductor films deposited on glass substrates for transparent electronics. J Non-Cryst Solids. 2006;352(23-25):2315-8.
- [63] Attia YA, Vázquez CV, Mohamed YM. Facile production of vitamin B 3 and other heterocyclic carboxylic acids using an efficient Ag/ZnO/ graphene-Si hybrid nanocatalyst. Res Chem Intermed. 2017;43:203-18.
- [64] Camarillo R, Rincon J. Photocatalytic discoloration of dyes: relation between effect of operating parameters and dye structure. Chem Eng Technol. 2011;34(10):1675-84.
- [65] Fernandez-Perez A, Marban G. Visible light spectroscopic analysis of methylene blue in water; what comes after dimer? ACS Omega. 2020;5(46):29801-15.
- Liang JH, Han X. Structure-activity relationships and mechanism of [66] action of macrolides derived from erythromycin as antibacterial agents. Curr Top Med Chem. 2013;13(24):3131-64.
- [67] Mekky AE, Farrag AA, Hmed AA, Sofy AR. Preparation of zinc oxide nanoparticles using aspergillus niger as antimicrobial and anticancer agents. | Pure Appl Microbiol. 2021;15(3):1547-66.
- Alvarez-Peral FJ, Zaragoza O, Pedreno Y, Argüelles JC. Protective role of trehalose during severe oxidative stress caused by hydrogen peroxide and the adaptive oxidative stress response in Candida albicans. Microbiology. 2002;148(8):2599-606.
- He L, Liu Y, Mustapha A, Lin M. Antifungal activity of zinc oxide nanoparticles against Botrytis cinerea and Penicillium expansum. Microbiol Res. 2011:166(3):207-15.
- [70] Ahmad M, Ahmed E, Hong ZL, Khalid NR, Ahmed W, Elhissi A. Graphene-Ag/ZnO nanocomposites as high performance photocatalysts under visible light irradiation. J Alloys Compd. 2013;577:717-27.
- [71] Ahmad M, Ahmed E, Hong ZL, Xu JF, Khalid NR, Elhissi A, et al. A facile one-step approach to synthesizing ZnO/graphene composites for enhanced degradation of methylene blue under visible light. Appl Surf Sci. 2013 Jun 1;274:273-81.
- [72] Pyne S, Sahoo GP, Bhui DK, Bar H, Sarkar P, Samanta S, et al. Enhanced photocatalytic activity of metal coated ZnO nanowires. Spectrochim Acta Part A: Mol Biomol Spectrosc. 2012 Jul 1;93:100-5.
- Xu F, Yuan Y, Wu D, Zhao M, Gao Z, Jiang K. Synthesis of ZnO/Ag/ graphene composite and its enhanced photocatalytic efficiency. Mater Res Bull. 2013;48(6):2066-70.
- [74] Liu X, Pan L, Zhao Q, Lv T, Zhu G, Chen T, et al. UV-assisted photocatalytic synthesis of ZnO-reduced graphene oxide composites with enhanced photocatalytic activity in reduction of Cr (VI). Chem Eng J. 2012;183:238-43.

- [75] Xiong Z, Zhang LL, Ma J, Zhao XS. Photocatalytic degradation of dyes over graphene–gold nanocomposites under visible light irradiation. Chem Commun. 2010;46(33):6099–101.
- [76] Guettai N, Amar HA. Photocatalytic oxidation of methyl orange in presence of titanium dioxide in aqueous suspension. Part I: Parametric study. Desalination. 2005;185(1–3):427–37.
- [77] Sahel K, Perol N, Chermette H, Bordes C, Derriche Z, Guillard C. Photocatalytic decolorization of Remazol Black 5 (RB5) and Procion Red MX-5B – Isotherm of adsorption, kinetic of decolorization and mineralization. Appl Catal B: Environ. 2007;77(1–2):100–9.
- [78] Sawai J, Shoji S, Igarashi H, Hashimoto A, Kokugan T, Shimizu M, et al. Hydrogen peroxide as an antibacterial factor in zinc oxide powder slurry. J Fermentation Bioeng. 1998;86(5):521–2.